Check for updates

Received: 7 July 2023 | Accepted: 22 August 2023

DOI: 10.1002/pamm.202300260

RESEARCH ARTICLE

Fractures in glaciers—Crack tips and their stress fields by observation and modeling

Angelika Humbert[1,2] | **Dietmar Gross**[3] | **Rabea Sondershaus**[3] | **Ralf Müller**[3] | **Holger Steeb**[4] | **Matthias Braun**[5] | **Jörg Brauchle**[6] | **Karsten Stebner**[6] | **Martin Rückamp**[7]

[1]Alfred-Wegener-Institut Helmholtz Zentrum für Polar- und Meeresforschung, Bremerhaven, Germany

[2]Department of Geosciences, University of Bremen, Bremen, Germany

[3]Institute for Mechanics, Technical University of Darmstadt, Darmstadt, Germany

[4]Institute of Applied Mechanics, University of Stuttgart, Stuttgart, Germany

[5]Institut für Geographie, Friedrich-Alexander-Universität Erlangen-Nürnberg, Erlangen, Germany

[6]German Aerospace Center, Institute of Optical Sensor Systems, Berlin-Adlershof, Germany

[7]Bavarian Academy of Science and Humanities, Section Geodesy and Glaciology, Munich, Germany

Correspondence
Angelika Humbert,
Alfred-Wegener-Institut Helmholtz Zentrum für Polar- und Meeresforschung, Bremerhaven, Germany.
Email: angelika.humbert@awi.de

Funding information
Deutsche Forschungsgemeinschaft, Grant/Award Number: (501994052)

Abstract

High-resolution optical camera systems are opening new opportunities to study fractures in ice. Here, we present data obtained from the Modular Aerial Camera System camera system operated onboard of Alfred Wegener Institute Helmholtz Centre for Polar and Marine Research (AWI) polar aircraft in northeast Greenland in 2022. In addition, we are using optical and radar satellite imagery. The study area is the 79°N Glacier (Nioghalvfjerdsbræ, 79NG), an outlet glacier of the Northeast Greenland Ice Stream. We found that crack tips are exhibiting additional isolated cracks ahead of the main crack. Subsequent crack propagation is starting from those isolated cracks, leading to an advance of the crack, with bridges between crack faces. The bridges provide information of the episodic crack propagation. Fractures have typically a length scale of kilometers and the distance of crack faces is in the order of meters to tenths of meters. Fracture modes will be inferred from stress fields computed by an inverse modeling approach using the Ice Sheet and Sea Level System Model. To this end, a surface velocity field derived from satellite remote sensing is used for the optimal control method that constrains model parameters, for example, basal friction coefficient or rheology.

1 | INTRODUCTION

Fractures in glaciers play a major role in the dynamics of ice sheets: (i) they are leading to calving of icebergs, to break-up events and disintegration of floating glacier tongues or ice shelves; (ii) they facilitate drainage of supraglacial lakes and act as pathways of summer melt water to the ice sheet base, enhancing lubrication, thus leading to seasonal acceleration;

This is an open access article under the terms of the Creative Commons Attribution-NonCommercial-NoDerivs License, which permits use and distribution in any medium, provided the original work is properly cited, the use is non-commercial and no modifications or adaptations are made.
© 2023 The Authors. *Proceedings in Applied Mathematics & Mechanics* published by Wiley-VCH GmbH.

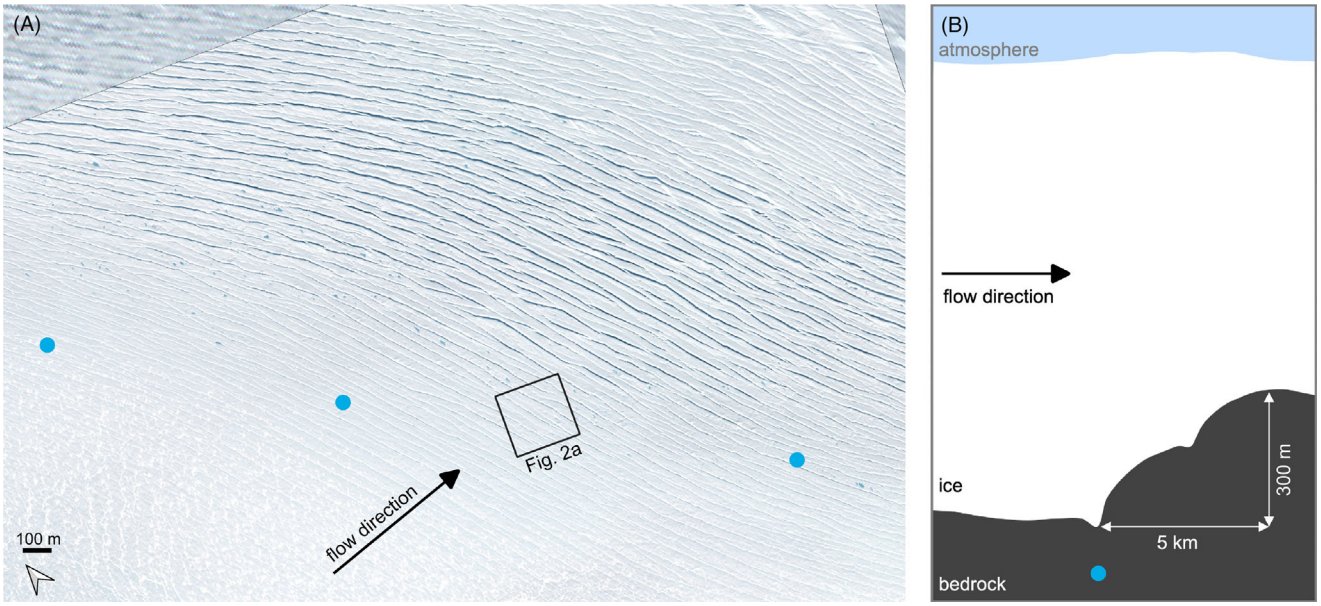

FIGURE 1 Panel (A) displays a crevasse zone of 79°N Glacier, Northeast Greenland. The high-resolution image is WV 2020-08-19, the background image Sentinel-2 2020-09-16. The blue dots denote steps in the bedrock topography. The square marks the area shown in Figure 2(A). Panel (B) shows a sketch of the geometry of the area based on radio echo sounding. A blue dot marks what the same symbol in the left panel is representing.

and (iii) fracture in the firn layer enables melt water percolation into subsurface layers, feeding water into aquifers some 10 m below the glacier surface.

The dynamics of ice sheets and glaciers is basically a gravity-driven lubricated flow. Ice obeys a viscoelastic Maxwell rheology with a nonlinear strain-rate-dependent viscosity [1]. Ice exhibits brittle behavior in the load situations typical for glaciers and ice sheets [2]. Due to geothermal and strain heating the base of ice sheet is over vast areas at the pressure melting point, leading to sliding. In the outlet glaciers, the velocity of the glacier is thus governed by sliding. Changes in the basal topography, for example, subglacial hills, are leading to changes in the glacier stress field, which leads to an increase in elastic strain. As a consequence, fractures are forming from the surface into the glacier. Their horizontal dimension is in the order of hundreds of meters to several kilometers in length and decimeters to tenths of meters of in width. The vertical extent is difficult to assess. Crack propagation is episodic, and is typically detected by massive changes in crack length between two satellite image acquisitions.

Although optical and radar satellite imagery has developed in the past decades in spatial and temporal resolution, the current standard 10 m resolution of Copernicus Sentinel-2 is not sufficient for studying the details of crack tip fields. Very high-resolution optical imagery, with pixel size of about 30 cm, is necessary to observe the details of crack tips. In our study, this is facilitated by two types of sensors: the optical satellite WorldView (WV, pan-chromatic and monochromatic) and the Modular Aerial Camera System (MACS) developed at the institute for optical sensors of the German Aerospace Centre operated on Alfred Wegener Institute's polar aircrafts.

This text is organized as follows: First, we present observations observation of crack fields, subsequently the stress field is discussed. Finally, the released energy by crevasse formation is presented, before we discuss our findings and draw conclusions.

2 | OBSERVATION OF CRACK FIELDS

First, the satellite imagery of the crevasse field is presented: the WorldView scene used here is acquired on 2020-08-19 and both the multichromatic image with 1.2 m resolution as well as the pan-chromatic image in 30 cm resolution are used. The area shown in Figure 1(A) is densely covered with fractures and coincides with a step in the bedrock topography. The onset of the step is detected from airborne radio echo sounding data and is marked with blue dots. The cracks are aligned parallel to the bedrock step and perpendicular to the flow direction marked with an arrow in Figure 1(A). Figure 1(B) displays a vertical profile of the glacier showing the step of about 300 m height in the bedrock over a distance of 5 km.

16177061, 2023, 3, Downloaded from https://onlinelibrary.wiley.com/doi/10.1002/pamm.202300260 by Dtsch Zentrum F. Luft-U. Raum Fahrt In D. Helmholtz Gemein., Wiley Online Library on [02/11/2023]. See the Terms and Conditions (https://onlinelibrary.wiley.com/terms-and-conditions) on Wiley Online Library for rules of use; OA articles are governed by the applicable Creative Commons License

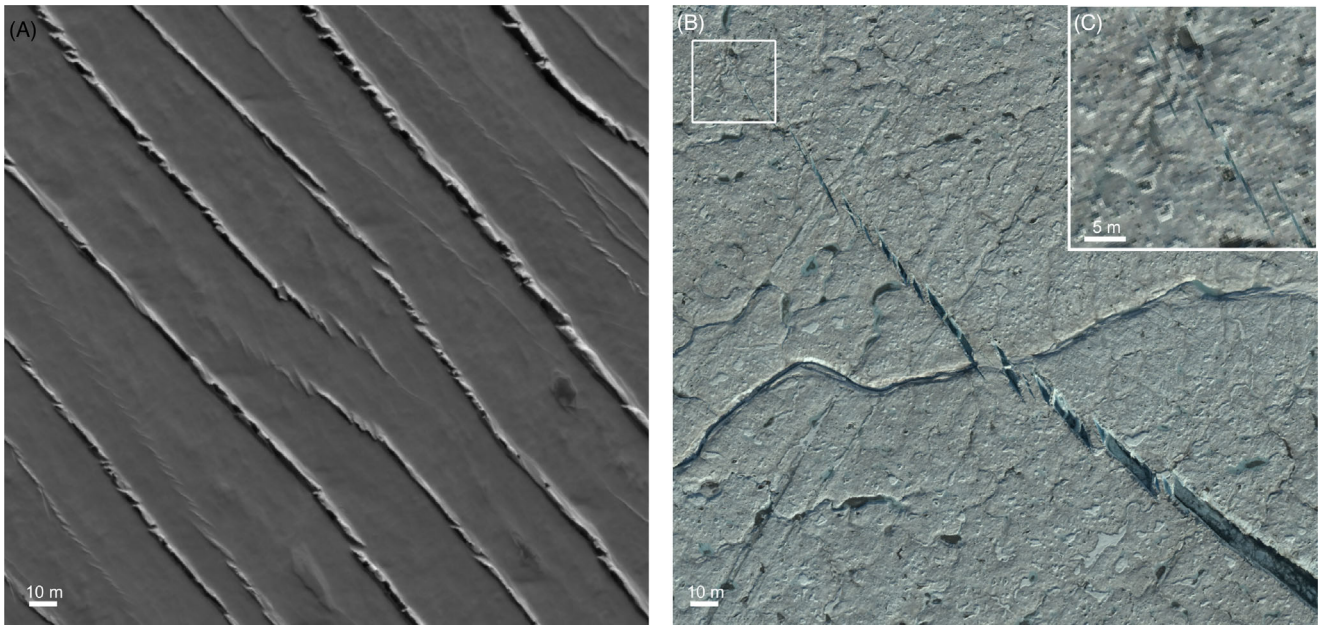

FIGURE 2 Panel (A) shows a subset of the crevasse field from Figure 1, but here the pan-chromatic mode of WV is used. Panel (B) displays a crevasse tip field acquired with the MACS system. Note that the area shown is not the same, but the scales of (A) and (B) are the same. Panel (C) is a zoom into the area of the white box in Panel (B).

The depth of the cracks is constrained from ice penetrating airborne radar: we have operated AWI's ultrawide band (UWB) radar onboard of Polar 5 in July 2021 and crossed the crevasse field. The resolution in the upper tenths of meters is not optimal, but the radio echo sounding data do not contain hyperbolas, which are typical for point reflectors such as crack fronts occurring below 20 m. Therefore, the cracks occur within the first meters of the glacier thickness. As the glacier has a thickness of around 1200 m at this location, the cracks are surface cracks.

Figure 2(A) displays a high-resolution pan-chromatic image of a subset of the crevasse field, as shown in Figure 1. Interestingly, many crack tips possess a field of tiny cracks in an angle of 45° to the main crack propagation direction. In order to discover if these tiny cracks also occur elsewhere, we employ high-resolution imagery from another side of the 79°N Glacier located close to the calving front. The data have been acquired with the MACS-Polar system during an airborne campaign at the end of the summer melt period; thus, no snow cover is left, which is an ideal condition for this purpose.

The MACS is an optical sensor instrument specifically developed for scientific application in unusual environment. It contains an RGB camera, as well as a near-infrared and thermal infrared camera, which were not used in this study. The flight was conducted 2022-08-20 over the 79°N Glacier. The aircraft was flying at an altitude of 1000 m above ground level, so that the optical configuration yields a ground sampling distance (GSD) of 0.15 m in the RGB and a swath width of 700 m. The MACS is a photogrammetric aerial camera, and thus, sensors are geometrically and radiometrically calibrated. In conjunction with the inertially aided georeferencing system, all necessary parameters of every pixel are known. The true orthophoto processing follows the common photogrammetric approach and with a given surface topography of the glacier, a mosaicing of the individual images is conducted. More details of the MACS-Polar system can be found in [3]. The resulting mosaic of a crack tip is presented in Figure 2(B).

Again, several tiny cracks are found in front of the main crack tip, in an angle of 45° to the main crack propagation direction. Due to glacier motion, the main crack widens. Thereby some of the connections between the crack faces will remain intact, while others will collapse or are close to failure. The intact connections forming small "bridges" between the crack faces, as sketched in Figure 3. The bridges can endure increasing displacements of the crack faces and slowly rotate due to the widening. To some extent, this behavior is captured in the high-resolution imagery from the calving front, see Figure 2(B), where the bridges reach a width of several meters. A more pronounced example than the one presented in this study is the so-called Halloween crack at the Brunt Ice Shelf,[1] Antarctica, where such a bridge has a width of 260 m up to 400 m.

[1] https://www.esa.int/ESA_Multimedia/Images/2017/02/Halloween_Crack

16177061, 2023, 3, Downloaded from https://onlinelibrary.wiley.com/doi/10.1002/pamm.202300260 by Dtsch Zentrum F. Luft-U. Raum Fahrt In D. Helmholtz Gemein., Wiley Online Library on [02/11/2023]. See the Terms and Conditions (https://onlinelibrary.wiley.com/terms-and-conditions) on Wiley Online Library for rules of use; OA articles are governed by the applicable Creative Commons License

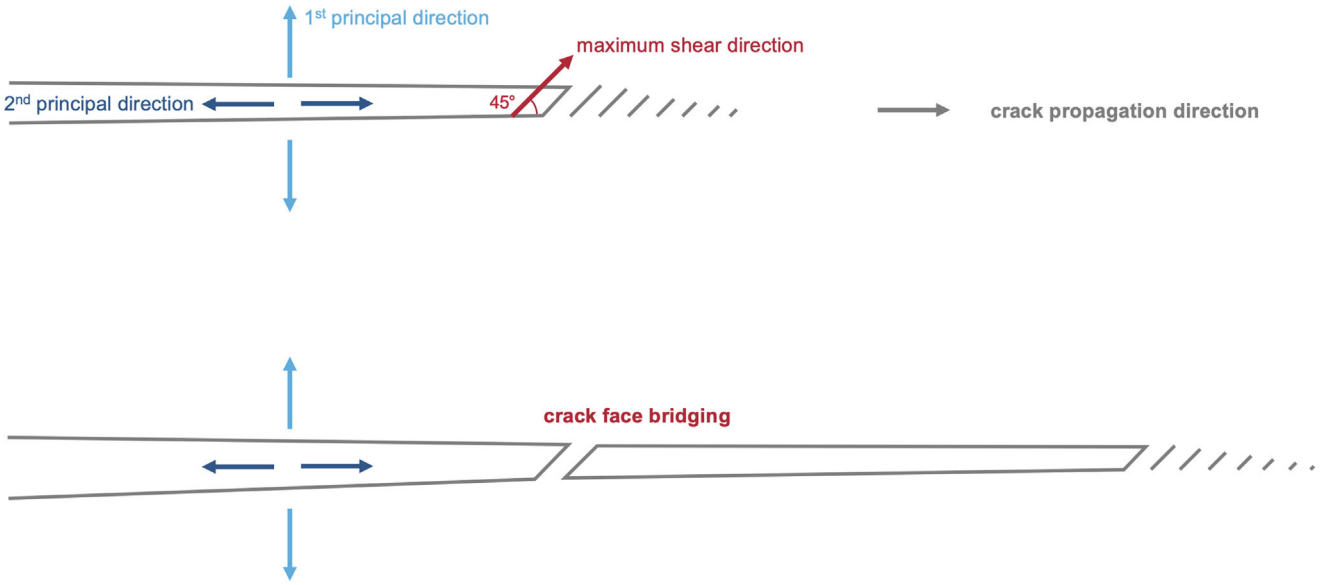

FIGURE 3 Sketch of the crack path evolution showing small cracks in front of the crack tip, inclined by 45° in the crack propagation direction and parallel to the maximum shear direction. As the crack evolves, a bridge between the crack faces remains and rotates due to the glacier motion.

3 | SIMULATED STRESS FIELD

To gain further insights into crack formation at the crevasse field, we investigate the principal stress fields at the surface of the glacier by means of an numerical model of ice flow dynamics. To represent the recent conditions, we conduct inverse modeling. Inverse modeling has become a standard approach in glaciological simulations to constrain the basal friction parameter, which is unknown due to inaccessibility.

We employ the Ice-sheet and Sea-level System Model (ISSM) [4] in the Blatter-Pattyn (BP) approximation for the ice dynamics [5, 6]. The modeling domain covers the whole drainage basin of the NEGIS catchment [7] with a variable horizontal resolution of the numerical mesh. The region of interest has a resolution of about 500 m. In the vertical direction, 15 layers refined toward the base are used. The ice geometry is taken from BedMachine v4 [8]. Within the optimization problem to infer the basal friction coefficient, a cost function is minimized by comparing modeled ice velocities with observed velocities [9]. To avoid overfitting or overregularization, an L-curve analysis was performed to select the optimal parameters for the inversion. From the modeled surface velocities, stresses are computed and the principal stresses are obtained together with their direction.

We display in Figure 4 the first and second principal stresses superimposed on the high-resolution imagery shown before, embedded in a low-resolution Sentinel-2 image of the area. The orientation of the simulated principal stresses matches the orientation of the cracks reasonably well. The first principal stress, plotted in light blue, is a tension stress and coincides with the perpendicular of the crack faces, whereas the second principal stress points in the direction of crack propagation. This indicates that the cracks were formed under mode I loading, which is characterized by a first principal tension stress perpendicular to the crack faces, whereas the second principal stress is in crack propagation direction. The direction of the maximum shear stresses is inclined by 45° to the principal stress directions. Consequently, we infer that the tiny cracks in front of the main crack tip and shifted by 45° are caused by locally high shear stresses and thus are formed under mode II loading.

A detailed analysis of the crack and the calving front (Figure 2B) was conducted in [3] and has shown that this crack is also a mode I crack. Therefore, it is comparable to the situation of the crevasse field.

4 | RELEASED ENERGY

We aim to estimate the energy that is released by fracture formation for a selected crevasse field. From satellite observations, we know that the onset of the crevasse field is not changing significantly over time. This is due to the fact that

16177061, 2023, 3, Downloaded from https://onlinelibrary.wiley.com/doi/10.1002/pamm.202300260 by Dtsch Zentrum F. Luft-U. Raum Fahrt In D. Helmholtz Gemein., Wiley Online Library on [02/11/2023]. See the Terms and Conditions (https://onlinelibrary.wiley.com/terms-and-conditions) on Wiley Online Library for rules of use; OA articles are governed by the applicable Creative Commons License

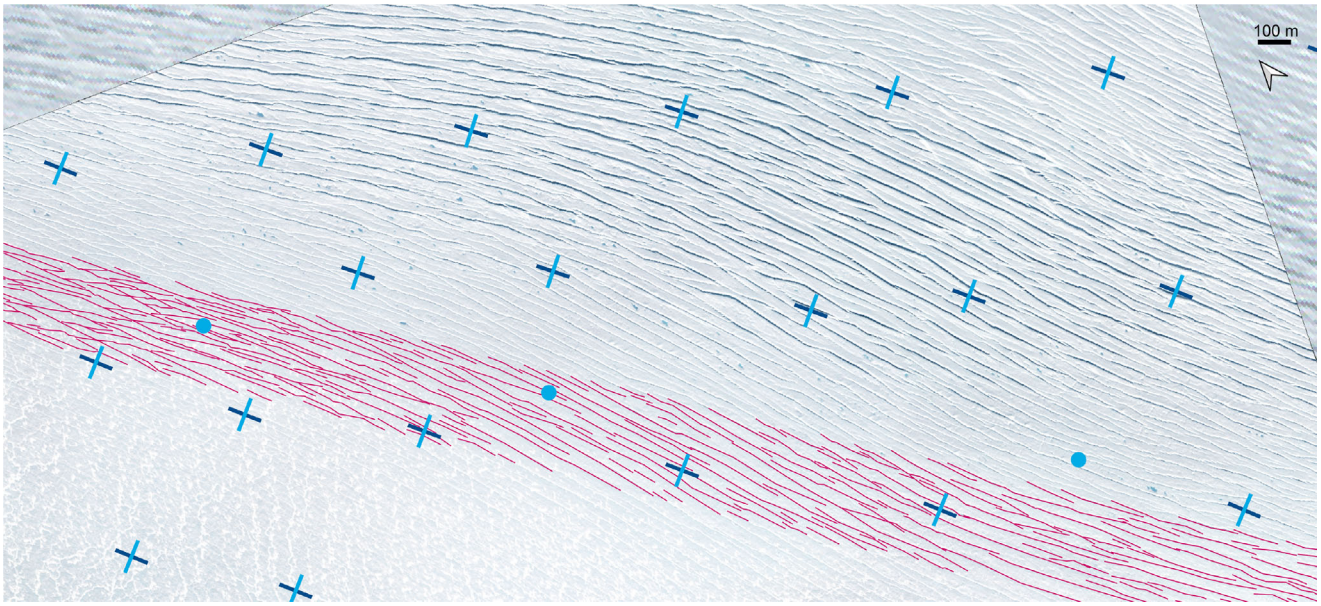

FIGURE 4 Orientation of the first and second principal stresses from inverse modeling, shown in light and dark blue, respectively, superimposed on top of the high-resolution (30 cm resolution) satellite imagery. The background image is a Sentinel-2 image in 10 m resolution.

the basal topography is the main cause of the tensile stresses leading to fracture formation. This allows us to estimate the area in which crevasses are formed each year, as the glacier velocity is known. Unfortunately, the high-resolution satellite imagery is only covering 65% of the entire area of the onset of the crevasse field. Thus, we scale our estimate up. Within the onset area of the crevasse field, we picked manually each crack path, so that the length of all cracks is known. The annual area containing new cracks is 2 497 032 m^2. The total sum of crack length within the 65% that is covered by the WorldView imagery is 67 490 m. As mentioned above, the crack depth is constrained to a maximum of 20 m. Therefore, we use for our estimate of the released energy 1–20 m as the crevasse depth. The critical energy release rate for plane strain situations is given by

$$\mathcal{G}_c = (1-\nu^2)\frac{K_{Ic}^2}{E} \tag{1}$$

with ν Poisson's ratio, E Youngs modulus, and K_{Ic} the fracture toughness. The plane strain assumption is justified, as the high contribution from sliding leads to a block motion in the upper part of the ice sheet. Poisson's ratio was assumed in other studies to be 0.325 [1]. The fracture toughness of polycrystalline ice has been measured to $K_{Ic} = 95.35 \pm 16.69\,\mathrm{kPa\,m^{1/2}}$ in a density range that is relevant for our area of application [10]. This leads to $\mathcal{G}_c = 8.131\,\mathrm{Jm^{-2}}$ assuming a Young's modulus of $E = 1$ GPa. For crack depth of 1, 2.5, 5, 10, and 20 m, we find $\Delta\mathcal{E} = \mathcal{G}_c\,\Delta A/2 = 0.8, 2.1, 4.2, 8.4, 16.8$ MJ, respectively. In this estimate, only main cracks, no tiny cracks, are considered, as many of them are buried under snow anyway. Therefore, we use MACS data (Figure 2B) to conduct a case study of one crack tip with numerous tiny 45° cracks. Here, we measured the crack length of each individual crack face. The summing up the length of all individual tiny cracks, we find with a total length of 767 m. Assuming again crack depth of 1, 2.5, 5, 10, and 20 m for the tiny cracks, we find $\Delta\mathcal{E}_{tiny} = \mathcal{G}_c\,\Delta A/2 = 6.2, 15.5, 31.1, 62.3, 124.7$ kJ. In the reference area, we tracked 303 cracks, and thus, we assume 606 tiny crack fields. Scaled to the entire annual area, this leads to 5.8, 14.5, 29.1, 58.1, and 116.3 MJ released energy for a crack depth of 1, 2.5, 5, 10, and 20 m, respectively.

5 | DISCUSSION

This study shows exemplary how beneficial high-resolution optical imagery is for conducting fracture mechanical analysis. We suggest to conduct similar studies at other locations, too, to benchmark our findings. Airborne data acquisition

16177061, 2023, 3, Downloaded from https://onlinelibrary.wiley.com/doi/10.1002/pamm.202300260 by Dtsch Zentrum F. Luft-U. Raum Fahrt In D. Helmholtz Gemein., Wiley Online Library on [02/11/2023]. See the Terms and Conditions (https://onlinelibrary.wiley.com/terms-and-conditions) on Wiley Online Library for rules of use; OA articles are governed by the applicable Creative Commons License

should focus on the onset of crevasse fields, where such tiny cracks are not yet covered with snow. Simulations as in [1] are ideal to identify suitable locations.

In our study, we solely investigated mode I cracks. A next step for a future study is to acquire data in areas, where it is a priori known that a shear situation takes place, such as shear margins of ice streams, preferably in their ablation zones at the end of the melt season, to obtain data of mode II cracks in high resolution.

When comparing the energy release by the main crack formation with the energy due to tiny cracks, we find that released energy due to the tiny cracks is a factor of 6.9 larger than the one from the main crack. In any energy estimate, it is thus important to consider them adequately.

From our estimate of the released energy of one single crevasse field, one could start to conduct this for the entire Greenland Ice Sheet to obtain an order of magnitude, based on the detection of all major crevasse areas given in [1].

As the major crevasse fields are formed in similar stress situations as considered here, we hypothesize that they are also primarily mode I cracks. This is also to be assessed in the future by means of observations and simulated stress fields. An advantage of the cracks being mainly formed by mode I cracks is that the laboratory measurements of mode I fracture toughness are a sufficient basis for estimates as conducted here.

Due to the enormous costs of optical satellite imagery, a machine learning approach is currently prohibited, but with a switch to open data policies, this would enable an entirely new way of conducting large-scale fracture analysis of ice sheets.

6 | CONCLUSIONS

We found tiny cracks in 45° orientation to the main crack ahead of the crack tip of mode I in many cracks in a crevasse field on a major Greenlandic outlet glacier. Cracks in 45° are presumably formed due to the maximum shear stress reaching a critical limit. Crack-face bridging was found to appear, with typical width of these bridges of about 3–6 m. This scale is likely to depend on the stress situations in which the crack is formed.

Simulated principal stress fields, based on inverse modeling, match very well the crack orientation. The use of observations of crack orientation as a benchmark for assessing simulations should be explored further in future.

As demonstrated in this case study, high-resolution optical imagery is the key for investigating crack evolution and propagation. In future, modeling-driven selection of survey sites will allow to acquire more data suitable for fracture mechanical analysis.

ACKNOWLEDGMENTS

The MACS data were acquired in the airborne campaign MACS@NG. We thank Gerit Birnbaum and Thomas Krumpen for conducting the flight in 2022. Radio echo sounding data were acquired during the 79NG-EC airborne campaign with AWI's Polar 5 in 2021. R.S. is supported by the Deutsche Forschungsgemeinschaft (DFG) under project 501994052 (MU 1370/21-1).

Open access funding enabled and organized by Projekt DEAL.

ORCID

Angelika Humbert https://orcid.org/0000-0002-0244-8760
Dietmar Gross https://orcid.org/0000-0001-9985-3668
Rabea Sondershaus https://orcid.org/0000-0001-6591-547X
Holger Steeb https://orcid.org/0000-0001-7602-4920

REFERENCES

1. Christmann, J., Helm, V., Khan, S. A., Kleiner, T., Müller, R., Morlighem, M., Neckel, N., Rückamp, M., Steinhage, D., Zeising, O., & Humbert, A. (2021). Elastic deformation plays a non-negligible role in Greenland's outlet glacier flow. *Communications Earth & Environment*, *2*(1).
2. Petrovic, J. (2003). Review mechanical properties of ice and snow. *Journal of Materials Science*, *38*, 1–6.
3. Humbert, A., Helm, V., Neckel, N., Zeising, O., Rückamp, M., Khan, S. A., Loebel, E., Gross, D., Sondershaus, R., & Müller, R. (2023). Precursor of disintegration of Greenland's largest floating ice tongue. *The Cryosphere*, *17*, 2851–2870.
4. Larour, E., Seroussi, H., Morlighem, M., & Rignot, E. (2012). Continental scale, high order, high spatial resolution, ice sheet modeling using the Ice Sheet System Model (ISSM). *Journal of Geophysical Research*, *117*(F1), F01022.

16177061, 2023, 3, Downloaded from https://onlinelibrary.wiley.com/doi/10.1002/pamm.202300260 by Dtsch Zentrum F. Luft-U. Raum Fahrt In D. Helmholtz Gemein., Wiley Online Library on [02/11/2023]. See the Terms and Conditions (https://onlinelibrary.wiley.com/terms-and-conditions) on Wiley Online Library for rules of use; OA articles are governed by the applicable Creative Commons License

5. Blatter, H. (1995). Velocity and stress fields in grounded glaciers: A simple algorithm for including deviatoric stress gradients. *Journal of Glaciology*, *41*(138), 333–344.
6. Pattyn, F. (2003). A new three-dimensional higher-order thermomechanical ice-sheet model: Basic sensitivity, ice-stream development and ice flow across subglacial lakes. *Journal of Geophysical Research*, *108*(B8), 2382.
7. Krieger, L., Floricioiu, D., & Neckel, N. (2020). Drainage basin delineation for outlet glaciers of northeast Greenland based on sentinel-1 ice velocities and tandem-x elevations. *Remote Sensing of Environment*, *237*, 111483.
8. Morlighem, M., Williams, C. N., Rignot, E., An, L., Arndt, J. E., Bamber, J. L., Catania, G., Chauché, N., Dowdeswell, J. A., Dorschel, B., Fenty, I., Hogan, K., Howat, I., Hubbard, A., Jakobsson, M., Jordan, T. M., Kjeldsen, K. K., Millan, R., Mayer, L., & Zinglersen, K. B. (2017). BedMachine v3: Complete bed topography and ocean bathymetry mapping of Greenland from multibeam echo sounding combined with mass conservation. *Geophysical Research Letters*, *44*(21), 11051–11061.
9. Joughin, I., Smith, B., Howat, I., & Scambos, T. (2015). Measures greenland ice sheet velocity map from insar data, version 2. National Snow and Ice Data Center.
10. Christmann, J., Müller, R., Webber, K. G., Isaia, D., Schader, F. H., Kipfstuhl, S., Freitag, J., & Humbert, A. (2015). Measurement of the fracture toughness of polycrystalline bubbly ice from an antarctic ice core. *Earth System Science Data*, *7*(1), 87–92.

How to cite this article: Humbert, A., Gross, D., Sondershaus, R., Müller, R., Steeb, H., Braun, M., Brauchle, J., Stebner, K., & Rückamp, M. (2023). Fractures in glaciers—Crack tips and their stress fields by observation and modeling. *Proceedings in Applied Mathematics and Mechanics*, *23,* e202300260. https://doi.org/10.1002/pamm.202300260

16177061, 2023, 3, Downloaded from https://onlinelibrary.wiley.com/doi/10.1002/pamm.202300260 by Dtsch Zentrum F. Luft-U. Raum Fahrt In D. Helmholtz Gemein., Wiley Online Library on [02/11/2023]. See the Terms and Conditions (https://onlinelibrary.wiley.com/terms-and-conditions) on Wiley Online Library for rules of use; OA articles are governed by the applicable Creative Commons License